

A New Imaging Geometry Model for Multi-receiver Synthetic Aperture Sonar Considering Variation of the Speed of sound in Seawater

Nguyen Dinh Tinh and Trinh Dang Khanh

Faculty of Radio-Electronic Engineering, Le Quy Don Technical University, Hanoi, Vietnam

* Corresponding Author: Nguyen Dinh Tinh, tinhnd_k31@lqdtu.edu.vn

Received March 13, 2021; Revised ; Accepted ; Published

* Regular Paper

Abstract: This paper proposes a new imaging geometry model for multi-receiver synthetic aperture sonar (SAS). The model considers the change of the speed of sound in seawater, the effect of platform movement on the acoustic velocity vector (AVV), and the Doppler effect. Based on the proposed model, a solution to determine the phase distribution was generated to improve the SAS image quality. The simulation results demonstrate the merits of proposed model compared to the traditional models that consider the speed of sound in seawater as a fixed value, ignore the change of AVV during transmission, and suppress the Doppler effect.

Keywords: Synthetic aperture sonar (SAS), geometry model, sound velocity, Doppler effect, SAS image, beamforming

1. Introduction

Synthetic aperture sonar (SAS) is based on the coherent combination of received signals in successive pings (pulse repetition interval) when a sonar platform moves along a straight path. With this principle, SAS can generate a virtual aperture that is many times larger than the physical size to increase the along-track (azimuth) resolution [1, 2]. Thanks to the achievement of high resolution independent of both the range and frequency, SAS is widely used for many applications, such as searching for small objects, imaging of wrecks, underwater archaeology, and pipeline inspection [2, 3].

The working principle of SAS is similar to that of synthetic aperture sonar (SAR). However, the area mapping rate of SAS is lower than that of SAR because the speed of sound in seawater is much lower than the propagation speed of electromagnetic waves in air. To increase the area coverage rate, multi-receiver SASs configured with a transmitter (projector) and a receiver (hydrophone) array have been used commonly in SAS applications [3, 4].

It is challenging to construct a geometry model that completely describes the physical processes for SAS

imaging reconstruction due to the complicated configuration and challenges of navigation, sound velocity errors, topographic errors, vehicle stability, and shallow waters [5]. A conventional model uses phase center approximation (PCA), which considers a projector/hydrophone pair as an element at a central point of the two elements, which is used to simplify the calculation [6]. Due to the difference of propagation distance in these two cases, PCA error is generated when calculating the propagation time from the transmitter to a target and then back to the receivers, which causes degradation of the SAS image quality [7].

To reduce the PCA error, a geometry model was made to consider the platform motion during reception [7]. However, this model does not consider the change of the speed of sound in seawater according to depth, it ignores the change of the acoustic velocity vector (AVV) during transmission, and it suppresses the Doppler effect. With these limited conditions, the physical processes affecting the received signals are not considered completely.

This paper proposes an imaging geometry model for multi-receiver SAS that takes into account the change of the speed of sound according to depth, the change of AVV during transmission, and the Doppler shift. It is based on more complete consideration of the physical processes compared with conventional models. With these complete

descriptions, the proposed model can provide simulation data for researching and developing SAS image reconstruction algorithms. Based on the back projection algorithm (BPA) [8], the SAS image quality obtained with the proposed model can be improved compared with that derived from conventional models.

2. Proposal of Imaging Geometry Model for Multi-receiver SAS

Two-dimensional (2D) models including range dimension (depth) and azimuth dimension have been used widely in research to improve the along-track resolution for multi-receiver SAS [3, 7, 8]. In the depth dimension, the speed of sound in seawater is a nonlinear function of temperature, salinity, and depth [9]:

$$c = 1402.5 + 5T - 5.44 \times 10^{-2} T^2 + 2.1 \times 10^{-4} T^3 + 1.33S - 1.23 \times 10^{-2} ST + 8.7 \times 10^{-5} ST^2 + 1.56 \times 10^{-2} Z + 2.55 \times 10^{-7} Z^2 - 7.3 \times 10^{-12} Z^3 + 1.2 \times 10^{-6} Z(\Phi - 45) - 9.5 \times 10^{-13} TZ^3 + 3 \times 10^{-7} T^2 Z + 1.43 \times 10^{-5} SZ \quad (1)$$

where T is the temperature in $^{\circ}\text{C}$, Z is the depth in m, S is the salinity in ‰, and Φ is the geographic latitude in $^{\circ}$.

The dependence of the speed of sound in seawater on depth is also described by the sound velocity profile (SVP) [10] obtained by using sound velocity profilers. The variation of the speed of sound in seawater can be up to 2% over a typical depth profile [1, 5], which can cause defocus and degrade SAS image quality. To deal with these variations, phase gradient autofocus (PGA) or an average value of the speed of sound can be used for reconstructing SAS images [5, 11].

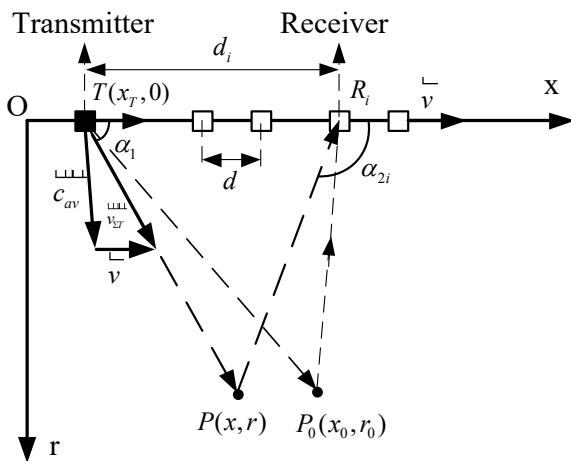


Figure 1. Geometry model of multi-receiver SAS

PGA is carried out based on acquisition data at receivers and phase adjustment according to neighbor points to achieve a sharp image. Therefore, it is difficult to construct mathematical models describing received signals and phase distribution using PGA. The proposed 2D

imaging geometry model for multi-receiver SAS is based on averaging the speed of sound along the depth combined with the consideration of the Doppler effect and the change of AVV during transmission, as shown in Fig. 1.

In Fig.1, c_{av} is the average speed of sound in seawater, and d is the distance between two adjacent elements in an array with N uniformly spaced receivers. The baseline distance between the transmitter and i th receiver is d_i . The SAS is moved along axis x with velocity v and is located at $O(0, 0)$ at $t = 0$. Axis r expresses the depth Z in (1) (it is also the range dimension [3, 7, 8, 13]).

The platform velocity vector can change due to rotational movements (pitch, roll, and yaw) and translational movements (heave, sway, and surge). These motions are accurately determined by high-grade aided inertial navigation systems (INSs), including an inertial measurement unit, Doppler velocity logger, and error state Kalman filter [5]. To obtain images with high quality, subwavelength navigation accuracy is required for reconstructing SAS images [14]. The requirement is satisfied by using the sonar itself as a navigation sensor combined with INS [5, 14]. Based on the navigation, the platform can be positioned, which is considered as a uniform velocity motion (speed v) to simplify SAS imaging reconstruction [3, 7, 8, 15, 17].

In Fig. 1, the total velocity vector $\vec{v}_{\Sigma T}$ is the sum of vectors \vec{v} and \vec{c}_{av} . The angle between $\vec{v}_{\Sigma T}$ and \vec{v} is α_1 [13]:

$$\alpha_1 = \arccos\left(\frac{x - vt}{\sqrt{(x - vt)^2 + r^2}}\right) \quad (2)$$

The module of the total velocity vector is expressed as:

$$v_{\Sigma T} = v \cos \alpha_1 + \sqrt{c_{av}^2 - v^2 \sin^2 \alpha_1} \quad (3)$$

The propagation time of the signal from the transmitter to point $P(x, r)$ is given by:

$$\tau_1 = \frac{\sqrt{(x - vt)^2 + r^2}}{v_{\Sigma T}} = \frac{\sqrt{(x - vt)^2 + r^2}}{v \cos \alpha_1 + \sqrt{c_{av}^2 - v^2 \sin^2 \alpha_1}} \quad (4)$$

After transmitting to point P , the signal is obtained at the i th receiver according to the direction from point P to receiver R_i , which is determined by angle α_{2i} :

$$\alpha_{2i} = \arccos\left(\frac{x - [d_i + v(\tau_1 + \tau_{2i}) + vt]}{\sqrt{[x - (d_i + v(\tau_1 + \tau_{2i}) + vt)]^2 + r^2}}\right) \quad (5)$$

The propagation time of the signal from P to R_i is τ_{2i} [13]:

$$\tau_{2i} = \frac{v\left(\sqrt{(x - vt)^2 + r^2} - (d_i + v\tau_1) \cos \alpha_1\right) + \sqrt{\Delta_i}}{c_{av}^2 - v^2} \quad (6)$$

where Δ_i is expressed as [13]

$$\Delta_i = v^2 \left(\sqrt{(x-vt)^2 + r^2} - (d_i + v\tau_1) \cos \alpha_1 \right)^2 + (c_{av}^2 - v^2) \left(\begin{array}{l} (x-vt)^2 + r^2 + (d_i + v\tau_1)^2 \\ -2\sqrt{(x-vt)^2 + r^2} (d_i + v\tau_1) \cos \alpha_1 \end{array} \right) \quad (7)$$

Types of signals used in modern SAS include gated continuous wave (CW), linear frequency modulation (LFM), and hyperbolic frequency modulation (HFM) pulses [11]. The CW pulse is widely used in classical sonar [1], whereas the LFM pulse is commonly used in modern SAS [3, 5, 7, 8, 11, 15]. Therefore, this section presents signal model for SAS using the CW pulse and LFM pulse. When using the CW pulse, the transmitted signal with carrier frequency f_c is expressed by:

$$s_e(\tau, t) = w(\tau) \exp(j2\pi f_c \tau) \quad (8)$$

where $w(\tau)$ is the windowing function of the transmitted signal (a Gaussian function or rectangle function). A rectangle function with pulse duration T_p is defined as [15]:

$$w(\tau) = \text{rect}\left(\frac{\tau}{T_p}\right) = \begin{cases} 1, & \left|\frac{\tau}{T_p}\right| \leq \frac{1}{2} \\ 0, & \text{otherwise.} \end{cases} \quad (9)$$

The received signal at point P is determined as:

$$s_p(\tau, t) = \omega_{TP}(t) w[\eta_1(\tau - \tau_1)] \times \exp\{j2\pi f_c [\eta_1(\tau - \tau_1)]\} \quad (10)$$

where $\omega_{TP}(t)$ is the beam pattern of the transmitter. η_1 is the time-stretching factor at point P due to the Doppler effect [16, 17]:

$$\eta_1 = \frac{c_{av}}{c_{av} - v \cos \alpha_1} \quad (11)$$

The received signal at the i th receiver due to the scattering from P is determined as:

$$s_i(\tau, t) = \omega_{TP}(t) \omega_{Ri}(t) w[\eta_1 \eta_{2i}(\tau - \tau_{2i}) - \eta_1 \tau_1] \times \exp\{j2\pi f_c \eta_1 \eta_{2i}(\tau - \tau_{2i}) - \eta_1 \tau_1\} \quad (12)$$

where $\omega_{Ri}(t)$ is the beam pattern of the i th receiver. η_{2i} is the time-stretching factor at the i th receiver due to the Doppler effect, which is calculated as [16, 17]:

$$\eta_{2i} = \frac{c_{av} + v \cos \alpha_{2i}}{c_{av}} \quad (13)$$

With the combination of received signals in the overlap of the main beams of the transmitter and each receiver,

$\omega_{TP}(t)$ and $\omega_{Ri}(t)$ can be suppressed to focus on the coherent processing of the phase. After ignoring the scattering from the sea surface, the received signal at the i th receiver is determined as:

$$s_i(\tau, t) = w[\eta_1 \eta_{2i}(\tau - \tau_{2i}) - \eta_1 \tau_1] \times \exp\{j2\pi f_c \eta_1 \eta_{2i}(\tau - \tau_{2i}) - \eta_1 \tau_1\} \quad (14)$$

When LFM pulses are used, the transmitted signal is expressed as:

$$s_{e_LFM}(\tau, t) = w(\tau) \exp(j2\pi f_c \tau + j\pi \gamma \tau^2) \quad (15)$$

where γ is the chirp rate [Hz/s]. Similarly to (14), the received signal at the i th receiver in SAS using the LFM pulses is given by:

$$s_{i_LFM}(\tau, t) = w[\eta_{2i}(\eta_1(\tau - \tau_{1i})) - \tau_{2i}] \times \exp\left\{ \begin{array}{l} j2\pi f_0 [\eta_{2i}(\eta_1(\tau - \tau_{1i})) - \tau_{2i}] \\ + j\pi \gamma [\eta_{2i}(\eta_1(\tau - \tau_{1i})) - \tau_{2i}]^2 \end{array} \right\} \quad (16)$$

Expressions (14) and (16) represent echo signals when considering the change of AVV during transmission, the Doppler effect, and the change of the speed of sound in seawater according to depth. Based on these equations, received data can be generated for researching and developing SAS imaging reconstruction algorithms.

3. Reconstructing SAS Image in Multi-receiver SAS Using BPA

SAS image reconstruction estimates the reflectivity function from backscattered echoes when an SAS platform moves along a known track [1, 2]. Due to its high resolution, BPA is implemented for SAS applications requiring image quality gain with arbitrary platform histories and a nonlinear SVP [4]. With the BPA, the image reconstruction in the range dimension and in the azimuth can be employed by a matched filter and beamforming, which is also called the delay-and-sum method [1, 2]. To evaluate the effectiveness of the proposed model, this section discusses SAS using the CW pulse for simplicity.

After match filtering, the pulse width at the output considered at half the level of the peak is equal to the pulse width of the CW pulse at the input. With wide CW pulses, the beamforming by the delay-and-sum method can be converted to the phase compensation after removing the carrier frequency. Based on the proposed model, the phase distribution is calculated as below when the main beam is steered to the target at point $P_0(x_0, r_0)$

$$\psi_i(t, x_0, r_0) = 2\pi f_c \left(\frac{c_{av}}{c_{av} - v \cos \alpha_{01}} \tau_{01} + \frac{c_{av} + v \cos \alpha_{02i}}{c_{av} - v \cos \alpha_{01}} \tau_{02i} \right) \quad (17)$$

where α_{01} and α_{02} are determined similarly to α_1 and α_2 in (4) and (5), but x and r are replaced by x_0 and r_0 , respectively. After compensating the phase, the backscattered signals from N receivers in M pings are coherently combined as:

$$ff(x, r, x_0, r_0) = \sum_{m=1}^M \sum_{i=1}^N ss_{eni}(\tau, t) \exp(j\psi_i(t, x_0, r_0)) \quad (18)$$

where $ss_{eni}(\tau, t)$ is the envelope signal obtained from (14) after demodulation.

The beam pattern in equation (18) is a function of the variables x and r , which are known as the azimuth slice when the range variable r is fixed [3, 7, 8, 13]. To reduce the side-lobe level (SLL) in the beam pattern, the elements in the receiver array must be arranged densely without gaps between two adjacent elements [1, 4]. With this condition, the main beam of each element is given by [18]

$$\beta_{0.5} = 1.22 \frac{\lambda}{d} \text{ (rad)} \quad (19)$$

For convenient calculation, this beam width can be approximately calculated as λ/d . The length of the synthetic aperture at range r was determined by [1]:

$$L_{sa} \approx r\eta \frac{\lambda}{d} \quad (20)$$

where η is a programmable parameter controlling the process beamwidth ($\eta \leq 1$) [1]. The number of pings for coherent processing according to the synthetic aperture length L_{sa} and the length of receiver array L is determined as:

$$M = \frac{L_{sa} - L}{v * T_i} \quad (21)$$

4. Simulation Results

To emphasize the effectiveness of the proposed model, we considered an example of multi-receiver SAS with the parameters shown in Table 1. These parameters were chosen to decrease SLL (the along-track sampling criterion) [1].

Table 1. The parameters of multi-receiver SAS

Parameters	Value	Unit
Carrier frequency (f_c)	100	kHz
Platform velocity (v)	2	m/s
Distance between the transmitter and the first receiver (d_i)	0.03	m
Distance between two adjacent receivers (d)	0.02	m
Number of receivers (N)	50	element
Pulse repetition interval (T_R)	0.2	s

SVP can be determined using accurate sound velocity profilers (e.g., *miniSVP* (www.valeport.co.uk), which has with an accuracy of 0.02 m/s). With this accuracy, SAS imaging reconstruction is implemented without correcting for sound velocity errors, in which case there are no accumulated errors from navigation inaccuracies [11]. When navigation errors are not compensated completely, the average sound velocity (ASV) for processing is chosen around the measured value until obtaining sharp images [11].

To focus on reconstructing SAS images, we used SSP from measured data [5, 11], as shown in Fig. 2, and we assumed that there are no navigation errors. Based on this SSP, the ASV between SAS and the seafloor is equal to 1492 m/s when the SAS is located at a depth of 4 m and the target is located on the seafloor with a depth of 17.3 m [11]. This ASV was used to generate SAS data. When the difference between the depth of the target and the depth of the SAS is calculated as 13.3 m, the number of pings M is 12 with $\eta = 0.6047$.

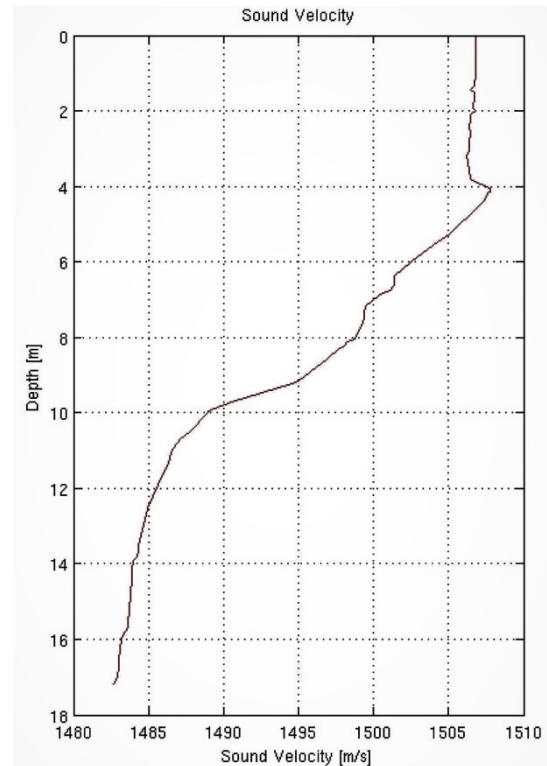


Figure 2. An example of SVP [5, 11]

To highlight the merits of the proposed model, we considered an ideal target located at (13.3 m; 2 m) in coordinate system O_{rx} . Azimuth slices were generated with MATLAB software, as shown in Fig. 3. There were three cases of beamforming based on the proposed model, the conventional model [8] ($c = 1500$ m/s, ignoring the change AVV and the Doppler effect), and PCA ($c = 1500$ m/s). In Fig. 3, the azimuth slices obtained from the proposed solution, the conventional solution [8], and the PCA are denoted by a solid red curve, dashed blue curve, and dotted brown curve, respectively.

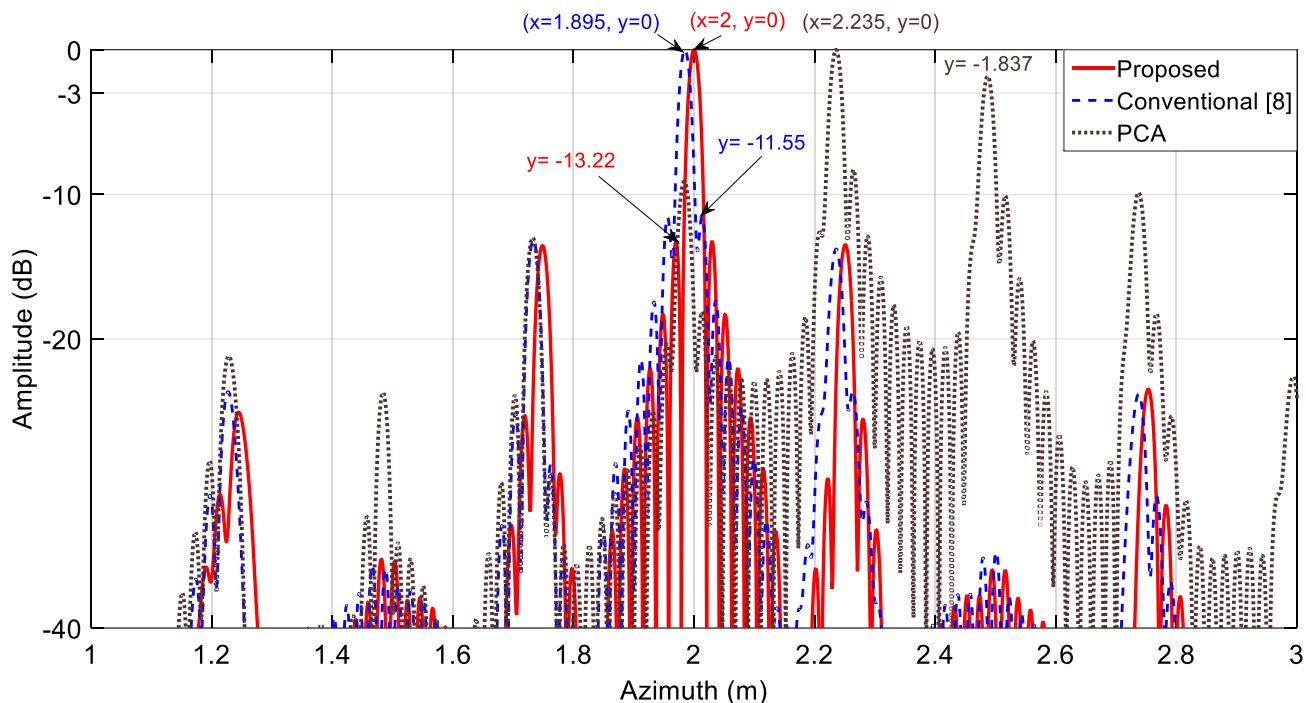


Figure 3. Azimuth slices of the point target at (13.3 m; 2 m)

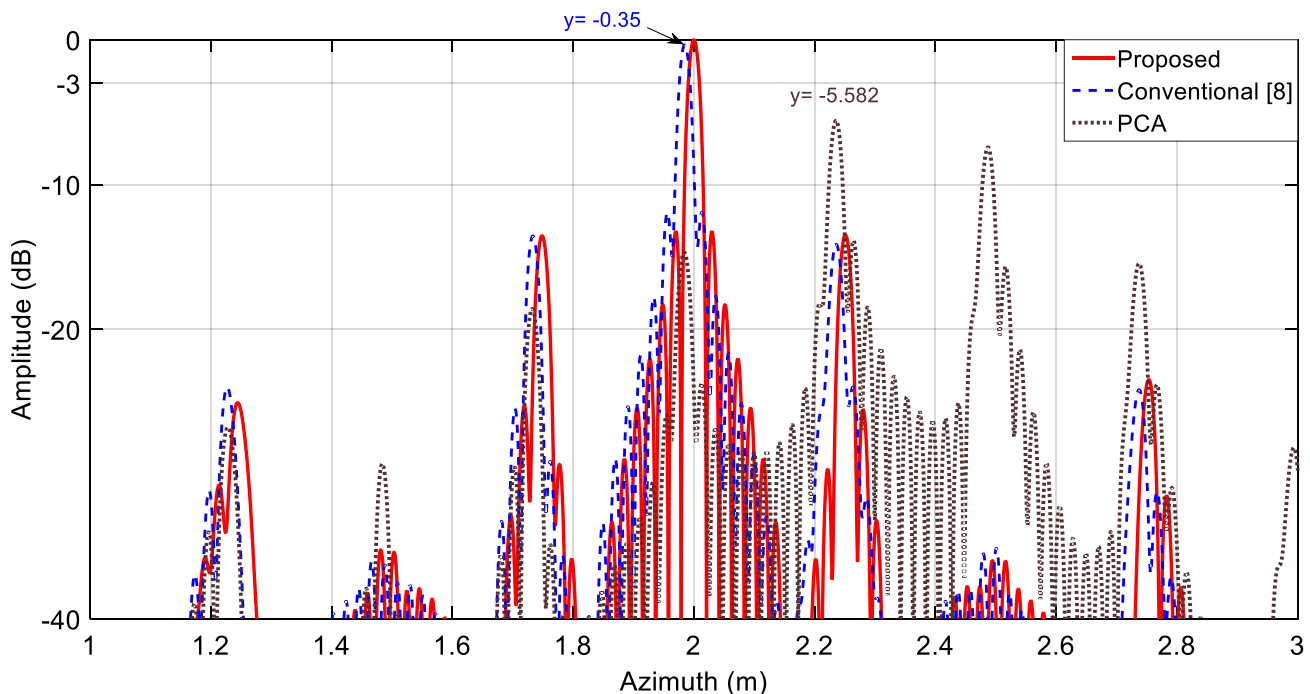


Figure 4. Relative normalized azimuth slices of the point target at (13.3 m; 2 m)

Fig. 3 shows that the proposed solution has no azimuth deviation. In cases of beamforming based on the conventional model [8] and PCA, the azimuth deviations are 0.105 m and 0.235 m, respectively. The deviations can cause defocus and degrade the image quality with distributed targets.

SLL in the azimuth slice derived from the proposed solution was also lower than that derived from the two conventional models. Compared with PCA, the proposed

solution generates a significantly lower SLL (11.383 dB). The improvement of SLL by the proposed solution in comparison with the conventional solution [8] is 1.67 dB. The improvements of SLL can increase the contrast of the SAS image and reduce reflections from the sea surface due to side lobes.

Fig. 4 shows the relative normalized azimuth slices obtained when the three azimuth slices in Fig. 3 are normalized according to the same maximum value (relative

normalization). The proposed solution increased the peak level of the main beam (or signal to noise ratio (SNR)) by 0.35 dB and 5.582 dB compared to the conventional solution and PCA, respectively. The improvement of SNR can increase the SAS imaging quality [19]. With the consideration of severe conditions, the computation time of the phase distribution using the proposed solution is larger than that using the conventional solution [8] and PCA. Table 2 shows the computation times based on MATLAB 2015A and a laptop with an i5-7200U Intel processor @ 2.5 GHz and 8 GB of RAM for the three cases with the target at (13.3 m, 2 m).

Table 2. The computation times of the phase distribution of the three solutions

PCA	Conventional [8]	Proposed
0.018 (s)	0.021 (s)	0.098 (s)

According to Table 2, the proposed solution uses more than 5 times and 4 times the computation time in comparison with the solution based on PCA and the conventional solution [8], respectively. To reduce the computation time, designers can use more powerful computing devices than ours. In addition to accurate sound velocity profilers, the proposed model required bathymetry equipment to map the scene prior to reconstructing SAS images, as in conventional SAS processing [1, 5, 11]. This requirement can be satisfied by accurate bathymetry equipment such as the MIDAS Surveyor

(www.valeport.co.uk) with accuracy being greater than ± 0.01 m or $\pm 0.02\%$.

For detection in the presence of multiple reflections (multipath), vertical SAS arrays are used for minimizing the seafloor-scattered echoes. With the configuration of the SAS array along the horizontal dimension used in this paper, multipath rejection was not implemented so as to concentrate on processing according to the azimuth dimension. This issue will be considered in more detail in the future.

5. Conclusion

This paper proposed a new imaging geometry model for multi-receiver SAS considering the variation of the speed of sound in seawater, the change of AVV during transmission, and the Doppler effect. From the proposed model, the SAS data could be generated to research and develop SAS image reconstruction algorithms. This paper also proposed a beamforming solution for multi-receiver SAS considering physical processes more completely than conventional models. With the proposed solution, the SAS imaging quality was improved by determining the target position more accurately, reducing SLL, and increasing SNR. The simulation results demonstrated the effectiveness of the proposed model and the merits of the proposed solution.

References

- [1] N. Kolev, "Sonar Systems", *InTech*, Croatia, pp. 3–25, Sep. 2011. [Article \(CrossRef Link\)](#)
- [2] R.E. Hansen, "Synthetic Aperture Sonar Technology Review," *Marine Technology Society Journal*, Vol. 47, No. 5, pp. 117-127, Oct. 2013. [Article \(CrossRef Link\)](#)
- [3] X. Zhang, et al., "An Imaging Algorithm for Multireceiver Synthetic Aperture Sonar," *Remote Sens*, 11(6):672, Mar. 2019. [Article \(CrossRef Link\)](#)
- [4] M. P. Hayes and P. T. Gough, "Synthetic Aperture Sonar: A Review of Current Status," in *IEEE Journal of Oceanic Engineering*, Vol. 34, No. 3, pp. 207-224, Jul. 2009, doi: 10.1109/JOE.2009.2020853. [Article \(CrossRef Link\)](#)
- [5] R. E. Hansen, et al., "Challenges in Seafloor Imaging and Mapping With Synthetic Aperture Sonar," in *IEEE Transactions on Geoscience and Remote Sensing*, vol. 49, no. 10, pp. 3677-3687, Oct. 2011, doi: 10.1109/TGRS.2011.2155071. [Article \(CrossRef Link\)](#)
- [6] A. Bellettini and M. A. Pinto, "Theoretical accuracy of synthetic aperture sonar microneavigation using a displaced phase-center antenna," in *IEEE Journal of Oceanic Engineering*, vol. 27, no. 4, pp. 780-789, Oct. 2002, doi: 10.1109/JOE.2002.805096. [Article \(CrossRef Link\)](#)
- [7] X. Zhang, et al., "Multireceiver Correction for the Chirp Scaling Algorithm in Synthetic Aperture Sonar," in *IEEE Journal of Oceanic Engineering*, vol. 39, no. 3, pp. 472-481, July 2014, doi: 10.1109/JOE.2013.2251809. [Article \(CrossRef Link\)](#)
- [8] X. Zhang, et al., "BP algorithm for the multireceiver SAS," *IET Radar Sonar Navig.*, Vol. 13, Nol. 5, pp. 830-838, May 2019. [Article \(CrossRef Link\)](#)
- [9] C. C. Leroy, "A new equation for the accurate calculation of sound speed in all oceans," *The Journal of the Acoustical Society of America*, Vol. 124, Nol. 5, pp. 2774-2782. Aug. 2008. [Article \(CrossRef Link\)](#)
- [10] P. C. Etter, "Underwater acoustic modeling and simulation," *CRC Press, 4th edition*, pp.30–35, Feb. 2013. [Article \(CrossRef Link\)](#)
- [11] R. E. Hansen, et al., "The SENSOTEK Synthetic Aperture Sonar: Results from HUGIN AUV trials," *Norwegian Defence Research Establishment*, pp. 11-21, June 2007. [Article \(CrossRef Link\)](#)
- [12] H. J. Callow, et al., "Stripmap phase gradient autofocus," *Oceans 2003. Celebrating the Past ... Teaming Toward the Future (IEEE Cat. No.03CH37492)*, San Diego, USA, 2003, pp. 2414-2421 Vol.5, doi: 10.1109/OCEANS.2003.178291. [Article \(CrossRef Link\)](#)
- [13] N. D. Tinh and T. Dang Khanh, "A New Imaging Geometry Model for Determining Phase Distribution in Multi-receiver Synthetic Aperture Sonar," *2019 6th NAFOSTED Conference on Information and*

Computer Science, Hanoi, Vietnam, 2019, pp. 518-521, doi: 10.1109/NICS48868.2019.9023897.
[Article \(CrossRef Link\)](#)

- [14] A. J. Hunter, et al., "Repeat-Pass Synthetic Aperture Sonar Micronavigation Using Redundant Phase Center Arrays," in *IEEE Journal of Oceanic Engineering*, vol. 41, no. 4, pp. 820-830, Oct. 2016, doi: 10.1109/JOE.2016.2524498. [Article \(CrossRef Link\)](#)
- [15] Y. Pailhas, et al., "Impact of temporal Doppler on synthetic aperture sonar imagery," *Journal of the Acoustical Society of America*, Vol. 143, Nol. 1, pp. 318 – 329. Jan. 2018. [Article \(CrossRef Link\)](#)
- [16] S Pinson, et al., "Relative velocity measurement from the spectral phase of a match-filtered linear frequency modulated pulse," *Journal of the Acoustical Society of America*, Vol. 140, Nol. 2, pp. 191-196, Aug. 2016. [Article \(CrossRef Link\)](#)
- [17] D. W. Hawkins and P. T Gough, "Temporal Doppler effects in SAS," Institute Of Acoustics Proceedings Vol. 26, Part 5, pp 1-10. [Article \(CrossRef Link\)](#)
- [18] G. Brooker, "Introduction to Sensors for Ranging and Imaging", SciTech, First edition, pp. 357-396, Jun. 2009. [Article \(CrossRef Link\)](#)
- [19] S. A. V. Synnes, et al., "Wideband Synthetic Aperture Sonar Backprojection With Maximization of Wave Number Domain Support," in *IEEE Journal of Oceanic Engineering*, vol. 42, no. 4, pp. 880-891, Oct. 2017, doi: 10.1109/JOE.2016.2614717. [Article \(CrossRef Link\)](#)



Nguyen Dinh Tinh received his B.E. degree in Electronics - Telecommunications and an M.E. degree in Radar Navigation Engineering from Le Quy Don Technical University, Vietnam, in 2008 and 2012, respectively. He has been working as a lecturer at Le Quy Don Technical University since 2009. His research interests include antennas, signal processing, synthetic aperture sonar, and sonar engineering.



Trinh Dang Khanh received his B.E. degree in Electronics - Telecommunications and Ph.D. degree in Electronic Engineering from Le Quy Don Technical University, Vietnam, in 1983 and 2000, respectively. He has been working as an Associate Professor since 2011 at Le Quy Don Technical University. His research interests include microwave circuit design, signal processing, inertial navigation system, and sonar engineering.